

Coexisting Kondo hybridization and itinerant f -electron ferromagnetism in UGe_2

Ioannis Giannakis¹, Divyanshi Sar¹, Joel Friedman¹, Chang-Jong Kang^{2,3}, Marc Janoschek^{4,a}, Pinaki Das^{4,b}, Eric D. Bauer⁴, Gabriel Kotliar^{2,7}, and Pegor Aynajian^{1*}

¹Department of Physics, Applied Physics and Astronomy, Binghamton University, Binghamton, New York 13902, USA

²Department of Physics and Astronomy, Rutgers University, New Jersey 08854, USA

³Department of Physics, Chungnam National University, Daejeon 34134, South Korea

⁴Los Alamos National Laboratory, Los Alamos, 87545, New Mexico, USA

⁵Condensed Matter Physics and Materials Science Department, Brookhaven National Laboratory, Upton, New York 11973, USA

^aPresent address: Laboratory for Neutron and Muon Instrumentation, Paul Scherrer Institute, Villigen PSI, Switzerland

^bPresent address: Advanced Photon Source, Argonne National Laboratory, 9700 S. Cass Ave, Lemont, IL 60439

* To whom correspondence should be addressed: aynajian@binghamton.edu

Kondo hybridization in partially filled f -electron systems conveys significant amount of electronic states sharply near the Fermi energy leading to various instabilities from superconductivity to exotic electronic orders. UGe_2 is a $5f$ heavy fermion system, where the Kondo hybridization is interrupted by the formation of two ferromagnetic phases below a 2nd order transition $T_c \sim 52$ K and a crossover transition $T_x \sim 32$ K. These two ferromagnetic phases are concomitantly related to a spin-triplet superconductivity that only emerges and persists inside the magnetically ordered phase at high pressure. The origin of the two ferromagnetic phases and how they form within a Kondo-lattice remain ambiguous. Using scanning tunneling microscopy and spectroscopy, we probe the spatial electronic states in the UGe_2 as a function of temperature. We find a Kondo resonance and sharp $5f$ -electron states near the chemical potential that form at high temperatures above T_c in accordance with our density functional theory (DFT) + Gutzwiller calculations. As temperature is lowered below T_c , the resonance narrows and eventually splits below T_x dumping itinerant f -electron spectral weight right at the Fermi energy. Our findings suggest a Stoner mechanism forming the highly polarized ferromagnetic phase below T_x that itself sets the stage for the emergence of unconventional superconductivity at high pressure.

Over the past decade, interest in exploiting ferromagnetic superconductivity with non-trivial topology dominated the field of quantum matter due to their robust functionalities in quantum information¹⁻³. Yet, quantum materials that exhibit natural coexistence of ferromagnetism and superconductivity remain rare. To date, only a handful of such synthesized single crystalline materials exist, with the majority being uranium-based heavy fermion compounds including UGe₂⁴, URhGe⁵⁻⁷, UCoGe⁸ and the recently discovered UTe₂⁹. In these compounds, the 5*f*-electrons play a critical role in the emergence of the exotic superconductivity¹⁰, making it particularly crucial to understand their controversial normal state behavior.

f-electrons in heavy fermion compounds exhibit dual characteristics of being itinerant and localized, driving an electronic competition between magnetism, very often of antiferromagnetic character, and heavy Fermi liquid behavior with quenched magnetic moments¹¹⁻¹⁵. Recent experimental and computational work demonstrated the dual nature of 5*f* electrons in USb₂^{16,17}, an antiferromagnetic heavy fermion system, through orbital selectivity, providing a natural explanation of how localized magnetism and itinerant heavy fermions of the same uranium 5*f* electrons coexist. The emergence of *f*-electron ferromagnetism and its interplay with Kondo coherence remains much less explored.

The ferromagnetic heavy fermion UGe₂ displays an interesting phase diagram^{5,18,19}. At ambient pressure, a second order paramagnetic-to-ferromagnetic phase transition at a relatively high $T_c \sim 52$ K¹⁸ is followed by a crossover meta-magnetic transition from a weakly polarized ferromagnetic state, FM1, to a strongly polarized ferromagnetic state FM2²⁰ at $T_x \sim 32$ K. Transport measurements show the emergence of the Kondo-lattice effect at $T_K \sim 110$ K, well above T_c ¹⁹. How the Kondo effect is impacted by the emergent ferromagnetism at and below T_c remains a question to be answered. Below T_c , specific heat measurements display a broad hump centered around T_x ^{19,21} which, along with magnetization measurements^{19,22} and neutron scattering²³ shows the presence of itinerant and localized subset of the uranium 5*f* electrons. In the same temperature range, Hall effect studies reveal a rapid increase of charge carriers below T_x suggestive of some sort of Fermi surface reconstruction²⁴. This reconstruction is argued to be caused by the sudden delocalization of the uranium 5*f* electrons. The microscopic origins of T_c and T_x are particularly important for the mechanism of emergent exotic superconductivity in UGe₂. With the application of hydrostatic pressure, the pressure-dependent FM2 transition line $T_x(P)$ decreases and terminates at the maximum of the emergent superconducting dome at $P_x \sim 1.2$ GPa, suggesting its fluctuations and destruction are directly related to the mechanism of superconductivity⁷. Furthermore, the superconducting dome only persists inside the FM1 phase, where both phases simultaneously disappear at the exact same pressure $P_c \sim 1.5$ GPa indicating an intimate relation between the ferromagnetism and superconductivity^{25,26}. Therefore, the emergence of itinerant 5*f*-electrons through the Kondo effect in UGe₂ and their evolution across T_c and T_x forms the low temperature normal state near the Fermi energy (E_F) out of which ferromagnetic superconductivity develops.

Theoretical understanding of the nature of the ferromagnetic state below T_x is controversial. One mechanism comes from the phenomenological ideas following the rigid-band Stoner approach,

where two sufficiently sharp and narrowly separated density-of-state peaks located near the Fermi energy form the majority and minority spin bands²⁷. Another idea involves charge and spin density waves emerging below T_x ¹⁸. In either case, direct experimental signature of a double peak structure or density waves have not been observed to date.

A sharp resonance in the density of states can naturally arise in heavy fermion compounds, whose energy relative to E_F depends on the valence of the f -electrons in the material system^{28,29}. Scanning tunneling microscopy (STM) has the spatial and energy resolution to probe the sharp resonance and its possible splitting³⁰. Yet, due to the lack of a natural cleaving plane in UGe_2 , which is crucial to obtain clean surfaces for STM, such an experiment have so far not been carried out. Here we use STM to probe the local electronic states and their temperature evolution near E_F in single crystal UGe_2 . We find multiple peaks in the density of states located near the chemical potential above T_c . The finding is in qualitative agreement with our DFT+Gutzwiller calculations presented here, attributing their origin to the different $5f$ -electronic orbital characters. With lowering of temperature, the two peaks located nearest to E_F strengthen and narrow. Below T_c and particularly near $T_x \sim 32$ K, the peaks split, forming additional kinks that further develop and evolve with temperature suggesting a Stoner mechanism of the ferromagnetic order. Our finding indicates a significant degree of itinerant character of the f -electrons through Kondo hybridization and the itinerant nature of the ferromagnetism involving the same f -electrons. At the lowest temperature, a sharp f -electronic density of states is formed at E_F setting the stage for the emergence of ferromagnetic spin-polarized superconductivity at higher pressure.

Figure 1a, b shows STM topographs of the (010) surface of single crystal UGe_2 , in-situ cleaved in our ultra-high vacuum, variable temperature STM. Cleaving exposes alternating terraces of two chemically different surfaces, termed A and B in Fig.1c. While surface A displays spatial uniformity with no atomic corrugation indicating the extended nature of the electronic states, surface B undergoes a surface reconstruction, whose quasiperiodic structure differs between different cleaves, as seen in Fig.1a, b. The asymmetry in the step height ($A \rightarrow B > B \rightarrow A$, with $A \leftrightarrow A = B \leftrightarrow B \equiv b$ -axis unit cell) between the different terraces allows us to compare the results to the crystal structure. Assuming only a single chemical bond breaking during the cleaving process leads us to identify surfaces A and B as uranium and germanium terminated, respectively (Fig.1c). Such an assumption is justified by the fact that only two surfaces have been observed based on ten different sample cleaves. The Ge surface with two Ge atoms per ac-plane unit cell, as compared to a single U or Ge atom per ac-plane for all other layers (see Fig.1), is also more likely to undergo surface relaxation and buckling. Nevertheless, the surface assignment here does not change the conclusions reached below.

STM spectra probed on the two surfaces just above T_c reveal two asymmetric low-energy peaks in the density of states in close proximity to the chemical potential, whose intensities are different on the two surfaces (Fig.1d). An additional broader high-energy peak near ~ 100 meV is also observed. Note that the intensity of the peaks on surface-B are spatially non-uniform and is further

elaborated below. At low temperatures (8 K), the low energy peaks undergo a splitting with the emergence of a kink/shoulder (Fig.1e). The high-energy peak remains mostly unchanged.

Peaks in the density of states near E_F is the hallmark of itinerant f -electron systems and have been seen in previous STM experiments in various $4f$ and $5f$ heavy fermions³¹. They are the results of the Kondo hybridization of localized f -orbitals with conduction electrons. To corroborate this observation, we compute the electronic structure of UGe_2 by employing the generalized gradient approximation to density functional theory (DFT) in combination with the Gutzwiller approximation (DFT+Gutzwiller)³². This method captures electronic correlations beyond the single-particle picture of DFT and has been successfully applied to other f -electron systems such as UO_2 ³³. The local Coulomb interaction strength and the Hund's coupling constant are $U = 6.0$ eV and $J = 0.57$ eV, respectively, for the correlated U $5f$ -orbital. The DFT+Gutzwiller calculations were performed at $T = 0$ K within the paramagnetic phase. Within DFT there is a significant mixing between U $5f_{5/2}$ and $5f_{7/2}$ states, so their spin-orbit splitting is not apparent. X-ray photoemission spectroscopy³⁴ and x-ray magnetic circular dichroism³⁵ measurements indicate that there is a clear spin-orbit splitting between U $5f_{5/2}$ and $5f_{7/2}$. Furthermore, the $5f_{5/2}$ level lies below the $5f_{7/2}$ level and the magnitude of the splitting is around 1.1 eV. This feature is well captured by the DFT+Gutzwiller calculations, which gives a spin-orbit splitting of ~ 1.5 eV. Our calculations indeed show multiple uranium $5f$ -electron peaks with different orbital character to reside near E_F (Fig.1f). More specifically, three major peaks located at energies of -18 meV, $+35$ meV and $+66$ meV that have characters of U ($J = 5/2$, $m_J = \pm 1/2, \pm 5/2, \pm 1/2$), respectively, are qualitatively consistent with the high temperature experimental data observed on surface A and/or B at ~ -20 meV, $\sim +25$ meV, and $\sim +100$ meV (Fig.1d, e).

While the relative widths and weights of the spectral lineshapes are spatially uniform on surface A (see Fig.2a), they vary significantly on surface B due to the structural inhomogeneity induced by surface reconstruction, as seen in Fig.2b. For example, looking at the different peaks, one can see that their intensity can be dramatically suppressed depending on the spatial location on the surface. This also applies to the spectra in Fig.1d, where at high temperature only the negative peak is observed with almost no peak intensity on the positive side. The disappearance of the positive bias peaks is due to the particular location of the spectrum on the surface and other locations (not shown here) do reveal a finite peak at positive and negative biases. This spatial variation renders studying the detailed temperature dependent evolution unreliable on surface B. We therefore focus on surface A (U surface) to probe the temperature dependence of the spectra across the two ferromagnetic transitions. Figure 3 shows our temperature dependent spectroscopy measurements carried out on surface A. The dI/dV conductance were measured in a constant current mode, I_{set} , and a bias voltage applied to the sample, V_{bias} , with a bias modulation of V_{mod} . Two sets of data with different experimental settings (energy-resolution) of $I_{set} = 150$ pA, $V_{bias} = 500$ meV, $V_{mod} = 5$ meV (Figure 3a) and $I_{set} = 1$ nA, $V_{bias} = 200$ meV, $V_{mod} = 1$ meV (Figure 3b) are shown. The spectra display an asymmetric resonance analogous to that seen in other heavy fermion systems^{31,36-41}. The observed resonance is the manifestation of Kondo hybridization,

delocalizing the f -electrons and merging them into the Fermi sea starting already at temperatures above T_c . As temperature is lowered below T_c , we observe the sharp kink at E_1 (near the Fermi energy) starting to develop particularly below ~ 35 K (see insets in Fig.3a, b). At the lowest measured temperature of 8 K, a clear double peak structure can be resolved with a peak separation ($E_1 - E_2$) of ~ 16 meV.

The strong temperature broadening of the spectral lineshapes makes it difficult to pin-point the onset of the E_1 kink in the raw data. In Fig.3c, d, we show the 2nd derivative of the spectral lineshapes, which highlights the kink-structure near the Fermi energy. While the temperature evolution is weak above ~ 35 K, it becomes more pronounced at lower temperatures. To better visualize this behavior, we contrast in Fig.3e, the high resolution spectra with a model Fano lineshape. A Fano lineshape in STM spectra resembles an asymmetric resonance peak due to interference between the two tunneling paths from the tip to the heavy (resonance) and light (continuum) electronic states of a Kondo lattice and has been widely used in STM analysis of heavy fermion systems⁴²⁻⁴⁶. The equation below represents the Fano lineshape

$$\frac{dI}{dV} \propto A \frac{\left(\frac{V-E}{\Gamma} + q\right)^2}{1 + \left(\frac{V-E}{\Gamma}\right)^2}$$

where E characterizes the resonance energy, Γ the resonance linewidth expressed as Half Width at Half Maximum (HWHM) and q is the tip-sample coupling, also known as the asymmetry parameter. A is related to the amplitude of the resonance. Figure 3e shows the data and the corresponding fit to a single Fano lineshape. We observe at 55K ($T > T_c$) that the data can be nicely modeled by a single resonance. At 35 K however, we can see that the data deviates from a single Fano lineshape particularly in the energy range of ± 10 meV, where a second resonance develops and grows stronger with further cooling. We therefore use a two Fano lineshape model (one centered at E_1 and another at E_2) to fit the temperature dependent data. Figure 4a shows the data together with their corresponding fit to the summation of two Fano resonances. For all temperatures, the model fit shows an excellent agreement with the data. No additional background is used in the model. The extracted resonance amplitude, widths, and energies are displayed in Fig.4 b, c, d respectively.

Looking at the amplitude of the resonances (Fig.4b), we first note that both resonances (E_1 and E_2) weaken with increasing temperature. While the E_2 resonance amplitude remains finite and large with no apparent anomaly at T_c , the E_1 resonance fades and within the experimental resolution becomes negligible above 35 K, as is reflected by the diverging error bars, which renders their values meaningless above 35 K. The extracted linewidths of the resonances also paint a similar picture. At the lowest temperature, the linewidths of the E_1 and E_2 resonances saturate at values of ~ 7 meV and ~ 13 meV, respectively. With increasing temperature, the E_2 resonance increases and within the experimental resolution follows the conventional temperature dependence expected in Kondo lattice systems $\Gamma(T) = \sqrt{(\pi k_B T)^2 + 2(k_B T_K)^2}$ ^{38,39}. Plotting $\Gamma(T)$ for a T_K of 110 K extracted from transport measurements (blue line in Fig.4c) reveals a good agreement with the

experimental data. On the other hand, the E_1 linewidths grow rapidly and diverge above 35 K, where the error bars span the entire y-range and the data are therefore omitted for $T > 35$ K from Fig.4c. The rapid decrease of spectral weight of the E_1 resonance together with its diverging linewidths with increasing temperature makes it difficult to ascertain its high-temperature evolution, particularly above 35 K. The extracted energies below 35 K show no significant temperature dependence.

We now turn to identify the origin of the observed double-peak structure at low temperatures. One possibility is the indirect Kondo hybridization gap⁴⁷. However, this scenario can be discarded in UGe_2 for two reasons. First, the observed band splitting occurs far below the Kondo lattice temperature of 110 K extracted from transport measurements. In fact, looking at the temperature dependence of the E_1 linewidth, one can see that it deviates dramatically from thermal broadening and $\Gamma(T)$ (red line in Fig.4c) and diverges near 35 K. Second, contrasting our observation in UGe_2 with the Kondo resonance in antiferromagnetic USb_2 ¹⁶, non-magnetic UTe_2 ⁹, and URu_2Si_2 ^{38,40} above its hidden order temperature, we see that all these uranium-based heavy fermion systems display a single Fano resonance above the chemical potential. Yet, none show a splitting or an indirect Kondo hybridization gap opening at low temperature, regardless of their magnetic or Kondo-coherence temperatures. Therefore, the splitting that we observe is likely not due to an indirect hybridization gap, which should show up similarly in these other U-based systems as well. We therefore turn to ferromagnetism as a possible origin of the band splitting (~ 16 meV) that we observe.

In itinerant ferromagnets, below their magnetic transition, the spin-majority and minority bands split due to the ferromagnetic exchange. Our observation is consistent with this Stoner mechanics of itinerant ferromagnetism. Indeed, the observation of a Kondo resonance above T_c and its further evolution below T_c provides spectroscopic evidence of the itinerant character of the f -electrons and therefore of the ferromagnetism in UGe_2 . This agrees with the fact that the ordered moment in the ferromagnetic phase is $1.4 \mu_B/U$, much smaller than the effective paramagnetic moment of $2.7 \mu_B/U$ ¹⁹. Evidence of itinerant ferromagnetism and band splitting is also seen in the optical spectroscopy of UGe_2 below T_c , where low energy excitations with an energy of $E \sim 13.6$ meV⁴⁸ have been observed. The latter is comparable to the separation of the E_1 - E_2 resonances seen here (Fig.4d). Similarly, a Stoner gap of the order of 40 K has also been inferred from magnetic neutron diffraction⁴⁹.

Overall, our data reveal a Kondo resonance with a characteristic Kondo-lattice temperature of 110 K, consistent with transport measurements¹⁹, that survives in the ferromagnetic phase. In heavy fermion systems, the magnetic ground state is generally in competition with the Kondo quenching of the magnetic moments that lead to the famous Doniach diagram. This holds true in Ce-based heavy fermions as seen in $CeRhIn_5$ and $CeCoIn_5$ ^{50,51}. In UGe_2 however, the two phenomena seem to coexist with no apparent competition, as seen by the largely unaffected Kondo resonance crossing T_c . A similar conclusion was reached in USb_2 ^{16,17}. Gradually below ~ 35 K, an additional kink/shoulder (E_1 resonance) develops that coincides with the highly polarized FM2 phase that

emerges as a crossover below $T_x \sim 32$ K. The E_1 resonance shifts the f -spectral weight closer to E_F , which leads to an enhanced electronic effective mass. The latter has been observed in the optical spectroscopy measurements⁴⁸. Hall measurements are also consistent with this picture, where a rapid increase of charge carriers indicating some sort of Fermi surface reconstruction is observed below T_x ²⁴. Altogether, these observations indicate the splitting of the resonance that likely onsets at T_c and becomes more pronounced below the crossover temperature T_x following the rigid band Stoner model^{27,49}, leading to a spin polarized f -electron band (E_1) at the Fermi energy, which sets the stage for a spin polarized superconductivity to emerge at high pressure. Future spin polarized STM study on the relative peak intensities of E_1 and E_2 will confirm the findings here, but is beyond the scope of this study.

1. Mackenzie, A. P. & Maeno, Y. The superconductivity of Sr₂RuO₄ and the physics of spin-triplet pairing. *Rev. Mod. Phys.* **75**, 657–712 (2003).
2. Sato, M. & Ando, Y. Topological superconductors: A review. *Reports Prog. Phys.* **80**, 076501 (2017).
3. Beenakker, C. W. J. Search for majorana fermions in superconductors. *Annu. Rev. Condens. Matter Phys.* **4**, 113–136 (2013).
4. Huxley, A. *et al.* UGe₂: A ferromagnetic spin-triplet superconductor. *Phys. Rev. B* **63**, (2001).
5. Saxena, S. S. *et al.* Superconductivity on the border of itinerant-electron ferromagnetism in UGe₂. *Nature* **406**, 587–592 (2000).
6. Aoki, D. *et al.* Coexistence of superconductivity and ferromagnetism in URhGe. *Nature* **413**, 613–616 (2001).
7. Aoki, D. & Flouquet, J. Superconductivity and Ferromagnetic Quantum Criticality in Uranium Compounds. *J. Phys. Soc. Japan* **83**, 61011 (2014).
8. Huy, N. T. *et al.* Superconductivity on the border of weak itinerant ferromagnetism in UCoGe. *Phys. Rev. Lett.* **99**, 067006 (2007).
9. Jiao, L. *et al.* Chiral superconductivity in heavy-fermion metal UTe₂. *Nature* **579**, 523–527 (2020).
10. Pfleiderer, C. Superconducting phases of f -electron compounds. *Rev. Mod. Phys.* **81**, 1551–1624 (2009).
11. von Lohneysen, H., Rosch, A., Vojta, M. & Wolfle, P. Fermi-liquid instabilities at magnetic quantum phase transitions. *Rev. Mod. Phys.* **79**, 1015–1075 (2007).
12. Si, Q. M. Quantum criticality and global phase diagram of magnetic heavy fermions. *Phys. Status Solidi B-Basic Solid State Phys.* **247**, 476–484 (2010).

13. Schroder, A. *et al.* Onset of antiferromagnetism in heavy-fermion metals. *Nature* **407**, 351–355 (2000).
14. Schröder, A., Aeppli, G., Bucher, E., Ramazashvili, R. & Coleman, P. Scaling of Magnetic Fluctuations near a Quantum Phase Transition. *Phys. Rev. Lett.* **80**, 5623–5626 (1998).
15. Zwicky, G. & Reese, M. Dual nature of strongly correlated 5f electrons. *J. Magn. Mater.* **310**, 201–206 (2007).
16. Ioannis Giannakis, Justin Leshen, Mariam Kawai, Sheng Ran, Chang-Jong Kang, Shanta R. Saha, Y. Zhao, Z. Xu, J. W. Lynn, Lin Miao, L. Andrew Wray, Gabriel Kotliar, Nicholas P. Butch, P. A. Orbital-selective Kondo lattice and enigmatic f electrons emerging from inside the antiferromagnetic phase of a heavy fermion. *Sci. Adv.* **5**, eaaw9061 (2019).
17. Chen, Q. Y. *et al.* Orbital-selective Kondo entanglement and antiferromagnetic order in $U\text{Sn}_2$. *Phys. Rev. Lett.* **123**, 106402 (2019).
18. Huxley, A. *et al.* $U\text{Ge}_2$: A ferromagnetic spin-triplet superconductor. *Phys. Rev. B* **63**, 144519 (2001).
19. Troc, R., Gajek, Z. & Pikul, A. Dualism of the 5f electrons of the ferromagnetic superconductor $U\text{Ge}_2$ as seen in magnetic, transport, and specific-heat data. *Phys. Rev. B* **86**, 224403 (2012).
20. Hardy, F. *et al.* Two magnetic Grüneisen parameters in the ferromagnetic superconductor $U\text{Ge}_2$. *Phys. Rev. B* **80**, 174521 (2009).
21. Palacio Morales, A. *et al.* Thermoelectric power quantum oscillations in the ferromagnet $U\text{Ge}_2$. *Phys. Rev. B* **93**, 155120 (2016).
22. Zhang, W., Liu, Y., Wang, X., Zhang, Y. & Xie, D. Strong coupling between localized 5f moments and itinerant quasiparticles in the ferromagnetic superconductor $U\text{Ge}_2$. *Chinese Phys. B* **27**, 037501 (2018).
23. Haslbeck, F. *et al.* Ultrahigh-resolution neutron spectroscopy of low-energy spin dynamics in $U\text{Ge}_2$. *Phys. Rev. B* **99**, 14429 (2019).
24. Tran, V. H., Paschen, S., Troc, R., Baenitz, M. & Steglich, F. Hall effect in the ferromagnet $U\text{Ge}_2$. *Phys. Rev. B* **69**, 195314 (2004).
25. Pfleiderer, C. & Huxley, A. D. Pressure Dependence of the Magnetization in the Ferromagnetic Superconductor $U\text{Ge}_2$. *Phys. Rev. Lett.* **89**, 147005 (2002).
26. Tateiwa, N. *et al.* Magnetic properties of a pressure-induced superconductor $U\text{Ge}_2$. *J. Phys. Soc. Japan* **70**, 2876–2879 (2001).
27. Sandeman, K. G., Lonzarich, G. G. & Schofield, A. J. Ferromagnetic superconductivity driven by changing Fermi surface topology. *Phys. Rev. Lett.* **90**, 167005 (2003).
28. Fisk, Z., Sarrao, J. L., Smith, J. L. & Thompson, J. D. The physics and chemistry of heavy fermions. *Proc. Natl. Acad. Sci. U.S.A.* **92**, 6663–6667 (1995).

29. Coleman, P. Heavy Fermions: electrons at the edge of magnetism. in *Handbook of Magnetism and Advanced Magnetic Materials* **1**, (J. Wiley and Sons, 2007).
30. Yazdani, A., Eduardo, H., Neto, S. & Aynajian, P. Spectroscopic Imaging of Strongly Correlated Electronic States. *Annu. Rev. Condens. Matter Phys.* **7**, 11–33 (2016).
31. Aynajian, P. *et al.* Visualizing Heavy Fermion Formation and their Unconventional Superconductivity in f -Electron Materials. *J. Phys. Soc. Japan* **83**, 061008 (2014).
32. Lanatà, N., Yao, Y., Wang, C., Ho, K. & Kotliar, G. Phase Diagram and Electronic Structure of Praseodymium and Plutonium. *Phys. Rev. X* **5**, 011008 (2015).
33. Yao, Y., Deng, X. & Kotliar, G. Slave Boson Theory of Orbital Differentiation with Crystal Field Effects : Application to UO₂. *Phys. Rev. Lett.* **118**, 126401 (2017).
34. Szajek, A., Che, G., Tro, R., Samsel-czeka, M. & Werwi, M. Intermetallics Electronic structure of UGe₂ at ambient pressure : Comparison with X-ray photoemission spectra. **19**, 1411–1419 (2011).
35. T. Okane., Kamoto, J. O., Amiya, K. M. Ujimori, S. F. *et al* Soft X-ray Absorption Magnetic Circular Dichroism Study of Ferromagnetic Superconductor UGe₂. *JSPJ* **75**, 024704 (2006).
36. Madhavan, V., Chen, W., Jamneala, T., Crommie, M. F. & Wingreen, N. S. Tunneling into a Single Magnetic Atom: Spectroscopic Evidence of the Kondo Resonance. *Science* **280**, 567–569 (1998).
37. Aynajian, P. *et al.* Visualizing heavy fermions emerging in a quantum critical Kondo lattice. *Nature* **486**, 201–206 (2012).
38. Aynajian, P. *et al.* Visualizing the formation of the Kondo lattice and the hidden order in URu₂Si₂. *Proc. Natl. Acad. Sci. U.S.A.* **107**, 10383 (2010).
39. Ernst, S. *et al.* Emerging local Kondo screening and spatial coherence in the heavy-fermion metal YbRh₂Si₂. *Nature* **474**, 362–366 (2011).
40. Schmidt, A. R. *et al.* Imaging the Fano lattice to ‘hidden order’ transition in URu₂Si₂. *Nature* **465**, 570–576 (2010).
41. Allan, M. P. *et al.* Imaging Cooper pairing of heavy fermions in CeCoIn₅. *Nat. Phys.* **9**, 468–473 (2013).
42. Maltseva, M., Dzero, M. & Coleman, P. Electron Cotunneling into a Kondo Lattice. *Phys. Rev. Lett.* **103**, 206402 (2009).
43. Figgins, J. & Morr, D. K. Differential Conductance and Quantum Interference in Kondo Systems. *Phys. Rev. Lett.* **104**, 187202 (2010).
44. Wölfle, P., Dubi, Y. & Balatsky, A. V. Tunneling into Clean Heavy Fermion Compounds: Origin of the Fano Line Shape. *Phys. Rev. Lett.* **105**, 246401 (2010).
45. Akbari, A., Thalmeier, P. & Eremin, I. Quasiparticle interference in the heavy-fermion superconductor CeCoIn₅. *Phys. Rev. B* **84**, 134505 (2011).

46. Coleman, P., Pépin, C., Si, Q. & Ramazashvili, R. How do Fermi liquids get heavy and die? *J. Phys. Cond. Matter* **13**, R723–R738 (2001).
47. Guritanu, V. *et al.* Optical spectra of the heavy fermion uniaxial ferromagnet UGe₂. *Phys. Rev. B* **78**, 172406 (2008).
48. Aso, N. *et al.* Stoner gap in the superconducting ferromagnet UGe. *Phys. Rev. B* **73**, 054512 (2006).
49. Knebel, G., Aoki, D. & Flouquet, J. Antiferromagnetism and Superconductivity in Cerium based Heavy Fermion Compounds. *C R Physique* **12**, 542 (2011).
50. Oppeneer, P. M. *et al.* Fermi surface changes due to localized–delocalized f-state transitions in Ce-115 and Pu-115 compounds. *J. Magn. Magn. Mater.* **310**, 1684–1690 (2007).

Acknowledgments

Work at Binghamton University is supported by the U.S. National Science Foundation (NSF) CAREER under award No. DMR-1654482. Work at Los Alamos National Laboratory was performed under the auspices of the US Department of Energy, Office of Basic Energy Sciences, Division of Materials Sciences and Engineering.

Author Contributions:

I.G. performed the STM measurements. I.G. and P.A. performed STM data analysis with help from D.S. and J.F.. C-J.K. and G.K. performed DFT + Gutzwiller calculations. M.J., P.D. and E.B. synthesized and characterized the materials. P.A. wrote the manuscript.

Figure captions:

Figure 1

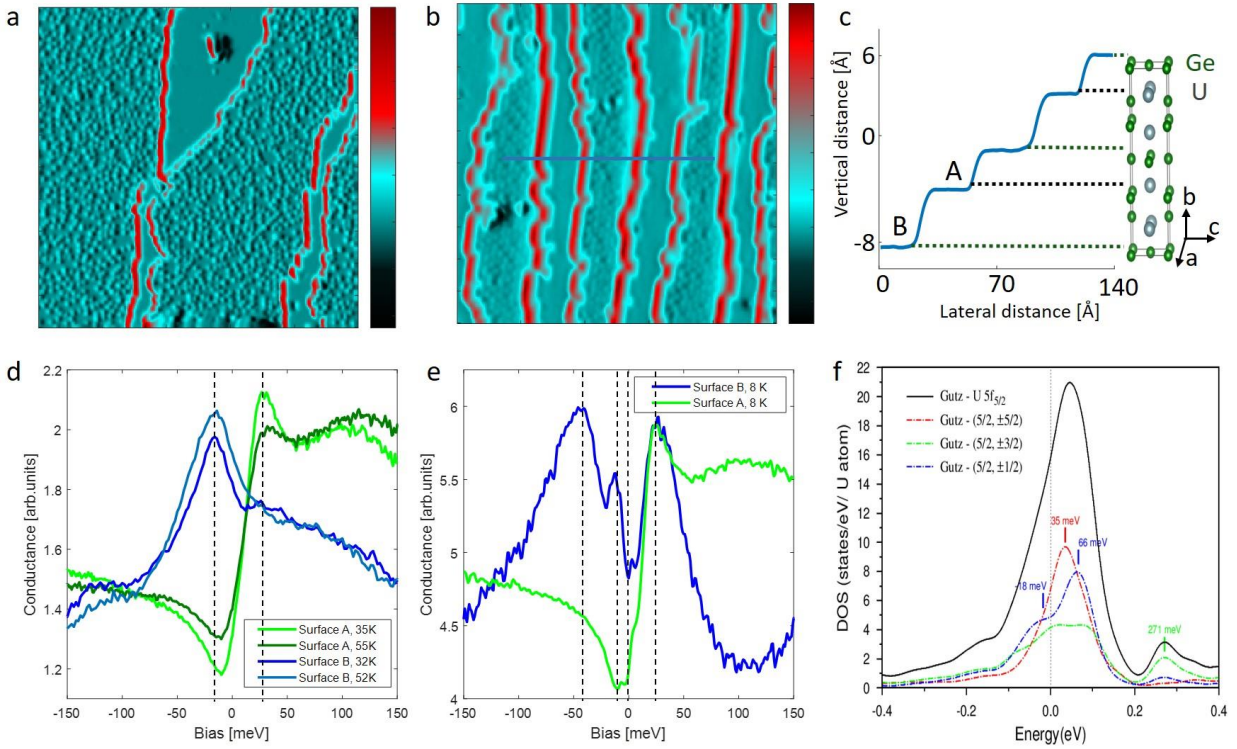


Figure 1: (a, b) Topographic image of cleaved UGe_2 revealing subatomic terraces with alternating chemically different surface terminations, one of which undergoes a surface reconstruction. (c) Comparison of the terrace heights extracted from the blue line-cut in (b) with the crystal structure of UGe_2 suggesting the breaking of a single bond ($U-Ge_2$) that exposes the reconstructed Ge_2 surface (B) and U surface (A). (d, e) STM dI/dV spectra on the two surfaces at high (d) and low (e) temperatures. Note that the data in (d, e) are not taken on the same spatial location. (f) DFT+Gutzwiller calculation of the electronic density of states in UGe_2 in the non-magnetic phase. Note that $U 5f_{7/2}$ due to spin-orbit coupling are at much higher energies (1 – 2 eV).

Figure 2

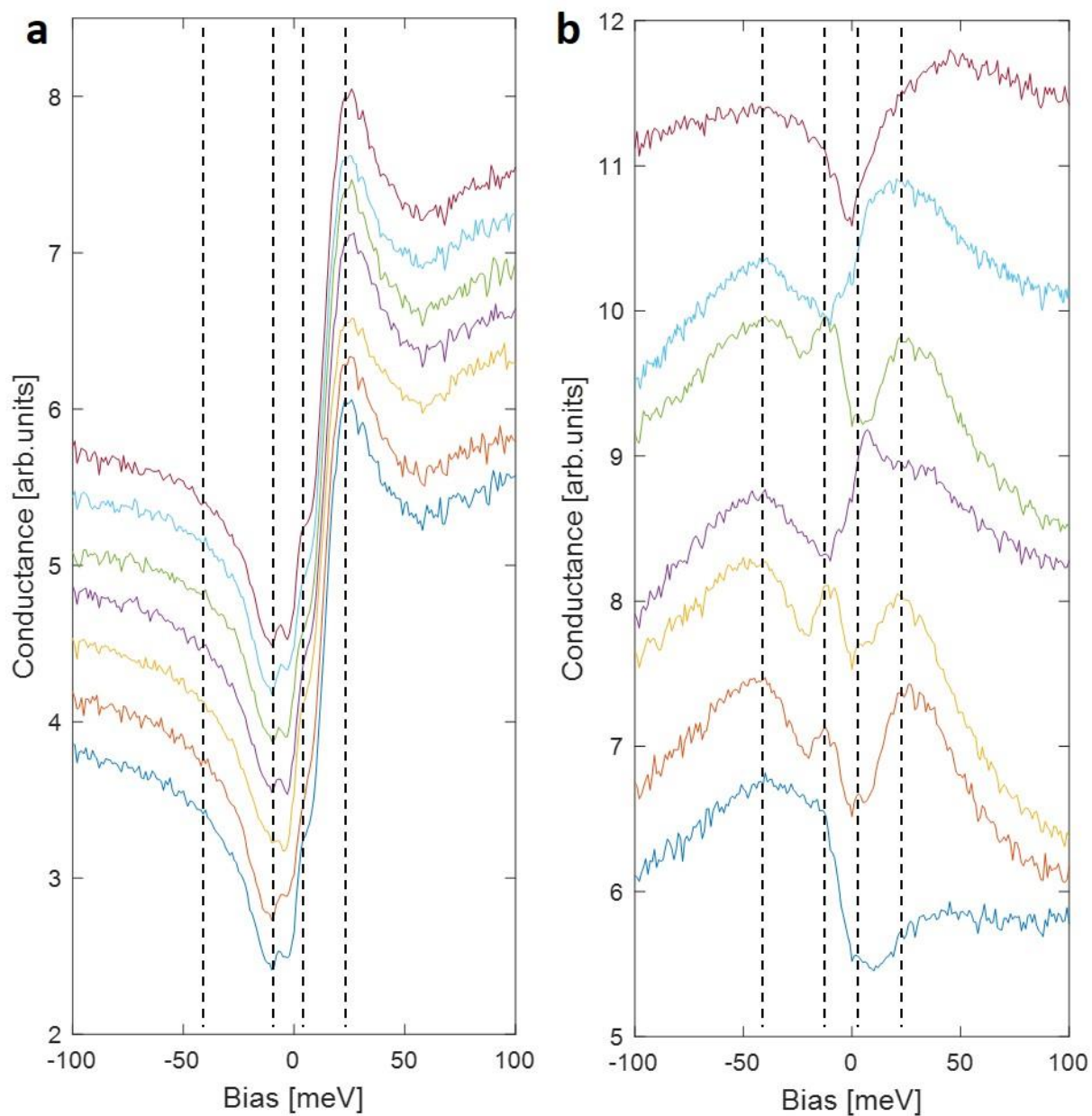


Figure 2: STM spectra taken at different locations on surfaces A (a) and B (b) at 8 K. The spectra in (a) reveal spatial uniformity, whereas those in (b) are spatially inhomogeneous due to the surface inhomogeneity. The lines correspond to the energies of the observed peaks that are similar on both surfaces.

Figure 3

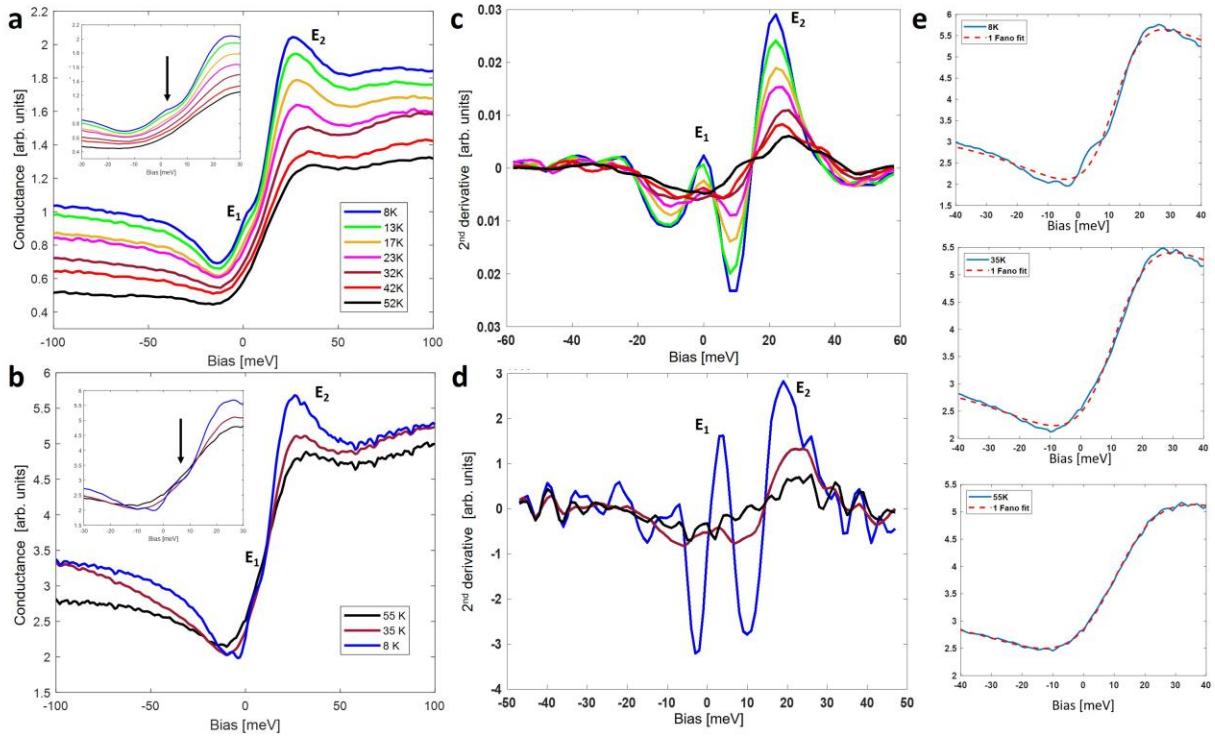


Figure 3: (a, b) STM spectroscopy on surface-A as a function of temperature with two different experimental settings described in the text. The spectra reveal a Fano lineshape (E_2 resonance) located above the chemical potential. As temperature is lowered below T_c , a second resonance emerges near the Fermi energy (E_1 resonance) below ~ 35 K. (c, d) Second derivative of the spectra in (a, b) showing the evolution of the E_1 and E_2 resonances as a function of temperature. (e) Fitting of the data in (b) to a single Fano lineshape. The spectrum above T_c can be explained by a single resonance, while at lower temperatures, the data deviates from a single Fano lineshape.

Figure 4

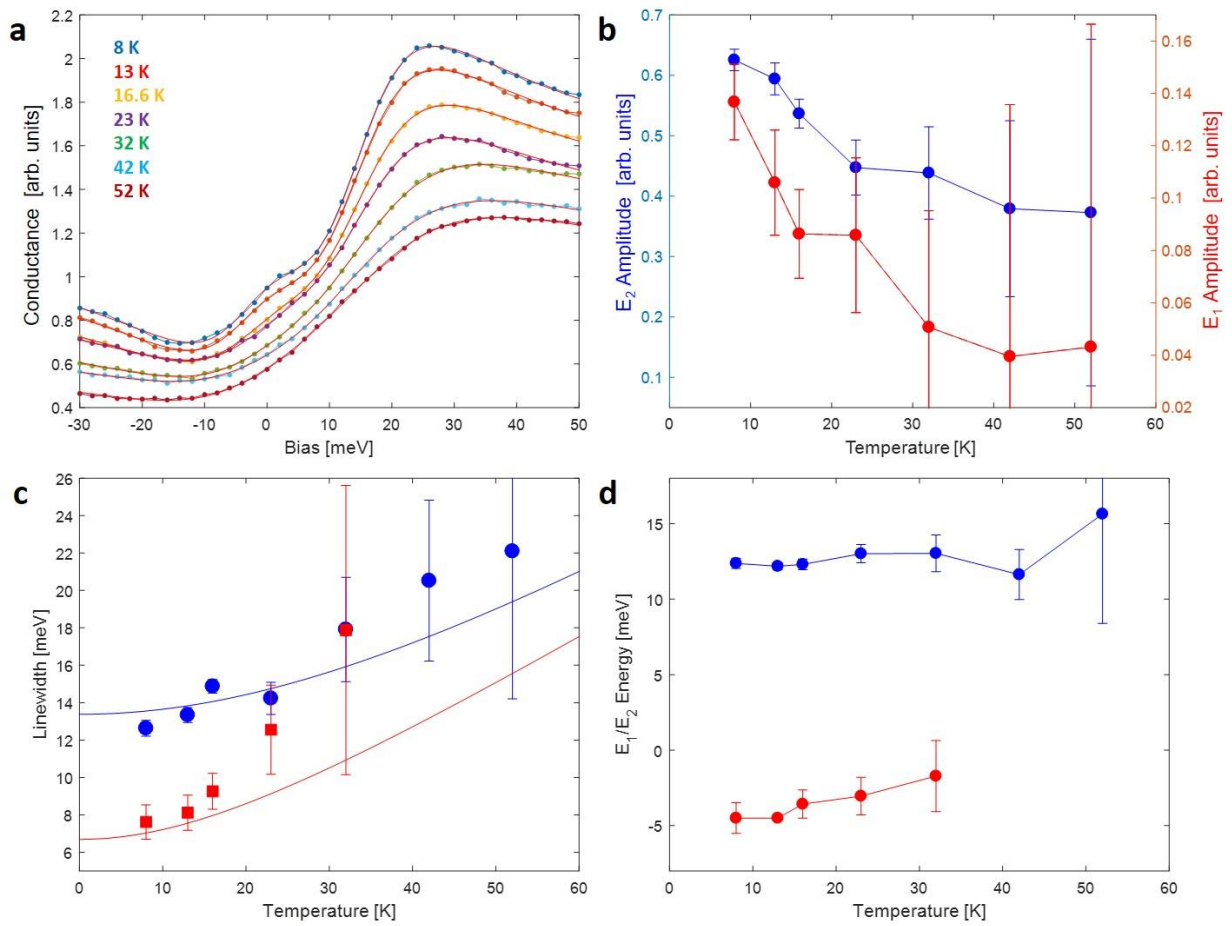


Figure 4: (a) STM spectroscopy and corresponding two Fano-lineshape model fit at different temperatures. (b,c,d) extracted Fano amplitude, width and energy as a function of temperature. Red data points correspond to the E_1 resonance near E_F whereas the blue data points correspond to the E_2 resonance above the chemical potential. The lines in (c) represent $\Gamma(T)$ for T_K of 110K (blue) and T_K of 55K (red).